Elliptic Feature of Coherent Fine Scale Eddies in Turbulent Channel Flows

Shin-Jeong Kang*, Mamoru Tanahashi, Toshio Miyauchi
Department of Mechanical and Aerospace Engineering, Tokyo Institute of Technology, Tokyo, Japan

Direct numerical simulations (DNS) of turbulent channel flows up to $Re_\tau=1270$ are performed to investigate an elliptic feature and strain rate field on cross sections of coherent fine scale eddies (CFSEs) in wall turbulence. From DNS results, the CFSEs are educed and the strain rate field around the eddy is analyzed statistically. The principal strain rates (i.e. eigenvalues of the strain rate tensor) at the CFSE centers are scaled by the Kolmogorov length η and velocity u_k. The most expected maximum (stretching) and minimum (compressing) eigenvalues at the CFSE centers are independent of the Reynolds number in each y^+ region (i. e. near-wall, logarithmic and wake regions). The elliptic feature of the CFSE is observed in the distribution of phase-averaged azimuthal velocity on a plane perpendicular to the rotating axis of the CFSE ($\boldsymbol{\omega}_c$). Except near the wall, phase-averaged maximum (γ^*/γ_c^*) and minimum (α^*/α_c^*) eigenvalues show maxima on the major axis around the CFSE and minima on the minor axis near the CFSE center. This results in high energy dissipation rate around the CFSE.

Key Words: Turbulent Channel Flow, Direct Numerical Simulations, Coherent Fine Scale Eddy, Scaling Law, Strain Rate Field

1. Introduction

It has been shown that turbulence consists of universal fine scale eddies (hereafter, coherent fine scale eddy (CFSE)) which are verified in homogeneous isotropic turbulence (Jimenez et al., 1993, 1998; Tanahashi et al., 1999, 2002a), turbulent mixing layer (Tanahashi et al., 2001) and turbulent channel flows (Tanahashi et al., 2004). The diameter and maximum azimuthal velocity of the CFSEs are scaled by the Kolmogorov length η and velocity u_k, respectively. The most expected diameter and maximum azimuthal velocity of the CFSEs are about 8η and $1.2u_k$ near the center of the channel, whereas they become about 10η and $2.0u_k$ in the near-wall region ($y^+<40$). These CFSEs are also associated with the intermittency of the dissipation rate of kinetic energy in turbulence.

From a previous study of strain rate acting on the CFSEs in turbulent mixing layer (Tanahashi et al., 2001), the eigenvectors of the minimum and maximum eigenvalues (α and γ) tend to be perpendicular to the rotating axis at the CFSE center ($\boldsymbol{\omega}_c$), and angles between this axis and the eigenvector of the intermediate eigenvalue (β) are less than 45° for about 70% of the CFSEs (Tanahashi et al., 2001). The most expected eigenvalue ratio becomes $\alpha:\beta:\gamma=-5:1:4$ at the CFSE center. In the near-wall turbulence, strain rate acting on the CFSE centers is slightly different from results of homogenous isotropic turbulence and turbulent mixing layer. The most expected eigenvalue ratio is $\alpha:\beta:\gamma=-7:1:6$ in the near-wall region, which indicates that large compression and stretching are acting on the CFSE centers near the wall (Tanahashi et al., 2004). In

* Corresponding Author,
E-mail: kang@navier.mes.titech.ac.jp
Department of Mechanical and Aerospace Engineering, Tokyo Institute of Technology, Tokyo, Japan. (Manuscript **Received** July 6, 2005; **Revised** December 30, 2005)

whole flow field, the eigenvector of β tends to be parallel to vorticity vector in the very near-wall region of turbulent channel flow (Blackburn et al., 1996 ; Tanahashi et al., 2004). Ashurst et al. (1987) and Soria (1994) have suggested that the eigenvalue ratio becomes $\alpha:\beta:\gamma=-4:1:3$ in regions of high energy dissipation rate in homogeneous isotropic turbulence, homogenous shear flows and turbulent mixing layer. In case of the CFSEs, the turbulent energy dissipation rate is quite small at the CFSE centers, but it is very large around the CFSEs (Tahanashi et al., 1996, 2001, 2002a). Therefore, the investigation of strain rate field on cross sections of the CFSEs may lead to the understanding of the energy dissipation mechanism.

Tanahashi et al.(1997, 1999) have reported that the mean azimuthal velocity profile of the CFSEs can be approximated by velocity distributions of a Burger's vortex which is an exact solution of Navier-Stokes equation. However, all characteristics of the CFSEs are not always approximated by axial symmetric Burger's vortex. Prochazka et al.(1998) have argued that the non-symmetric Burger's vortices under the strong strain can exist in turbulent flows quasi-steadily, and the streamlines and contours of their vorticity have elliptic feature. In homogeneous turbulence, the cross section of the CFSE shows distinct elliptic feature due to strain fields, and the large strain rate field and energy dissipation rate tend to be distributed around the CFSEs (Tanahashi et al., 2002a ; Miyauchi et al., 2002). In the near-wall region, since the strong mean shear exists and the most expected diameter and maximum azimuthal velocity of the CFSEs are larger than those in other turbulent flows, there is a possibility that elliptic feature and strain rate field on cross sections of the CFSEs are different from those in the outer layer or in other turbulent flows.

In the present study, direct numerical simulations of turbulent channel flows up to $Re_\tau=1270$ are conducted. The CFSEs are extracted from the DNS data. Reynolds-number dependence of the principal strain rates at centers of the educed CFSEs is investigated in the near-wall, logarithmic and wake regions. For $Re_\tau=800$, the elliptic feature and strain field on cross sections of the CFSEs are investigated in the near-wall region and in the outer layer by using a phase-averaging analysis.

2. DNS Database

New direct numerical simulations of $Re_\tau=400$ and 1270 have been performed in addition to $Re_\tau=800$ (Tanahashi et al., 2004). Here, Re_τ is the Reynolds number based on a friction velocity (u_τ) and a channel half width (δ) and the superscript $+$ denotes wall units. Spectral methods are used in the streamwise (x) and spanwise (z) directions, and the central finite difference method with fourth-order accuracy is used in the wall-normal (y) direction. The aliasing errors in the x- and z-directions are completely removed by using the 3/2 rule proposed by Orszag (1971). Periodic boundary conditions are used in the x- and z-directions for the velocity and pressure fields. No-slip condition is applied in the y-direction. Table 1 shows computational domain sizes (L_x, L_y, L_z), numbers of grid points (N_x, N_y, N_z) and spatial resolutions (Δx^+, Δy^+, Δz^+) in the x-, y- and z-directions.

Figure 1(a) shows profiles of the mean streamwise velocity ($\bar{u}^+$) for all Reynolds number cases. The solid and dashed lines in Fig. 1(a) represent the linear and the log law, respectively. The result for $Re_\tau=180$ is a good agreement with DNS result of Kim et al.(1987) who are using full spectral methods. There are roughly two regions,

Table 1 DNS database of turbulent channel flows

Re_τ	Re_c	u_τ	$L_x\times L_y\times L_z$	$N_x\times N_y\times N_z$	Δx^+	Δy^+	Δz^+
400	8200	0.0488	$3\pi\delta\times2\delta\times\pi\delta$	$384\times385\times192$	9.817	0.470～5.813	6.544
800	17760	0.0446	$2\pi\delta\times2\delta\times\pi\delta$	$512\times769\times384$	9.817	0.479～5.813	6.544
1270	30320	0.0417	$2\pi\delta\times2\delta\times\pi\delta$	$864\times1239\times648$	9.236	0.450～5.813	6.157

i.e. near-wall region (I) and outer layer (II). Curves in $y^+>40$ for $Re_\tau=400$, 800 and 1270 correspond with the solid line (log-law curve), and wake regions are clearly observed in approximately $y^+>200$ ($Re_\tau=400$) ~450 ($Re_\tau=1270$). Namely, the outer layer can be classified as the logarithmic and wake regions. Figure 1(b) shows budgets of the turbulent kinetic energy for $Re_\tau=180$ in wall units, i.e. each term is normalized with u_τ^4/ν. The DNS result of Mansour et al.(1988) is also plotted. Near the wall, the absolute values of the production and dissipation terms are very good agreement of those of Mansour et al.(1988).

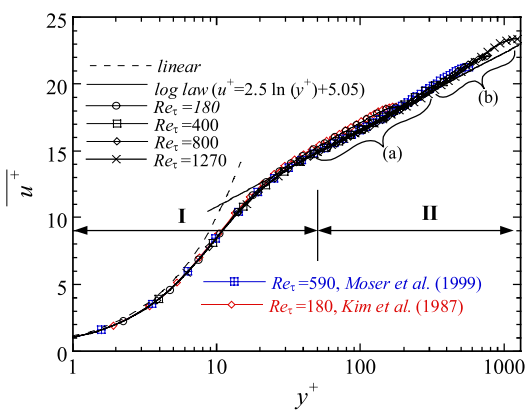

(a)

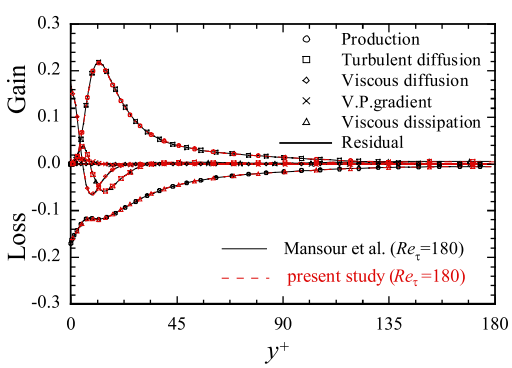

(b)

Fig. 1 (a) The distributions of the mean streamwise velocity for all Reynolds number cases. I: near-wall region, II: outer layer (logarithmic (1) and wake (2) regions). (b) The budgets of transport equation for the turbulent kinetic energy for $Re_\tau=180$

3. Strain Rate at CFSE Centers

Figure 2(a) shows iso-surfaces of the second invariant (Q; see Hunt et al., 1988; Tanahashi et al., 1999) of the velocity gradient tensor for $Re_\tau=400$. The visualized domain size is the lower half of the computational domain. This figure indicates that streamwise vortices in the near-wall region and hairpin-type vortices can be visualized by using the positive Q region. However, this visualization method depends on the threshold of Q. Therefore, in the present study, a new identification scheme (Tanahashi et al., 1999) based on a local flow pattern has been adopted to educe fine scale eddies without any threshold from the flow fields. The educed section includes a local maximum of Q along with the axis of a fine scale eddy, and a central point of swirling motion is

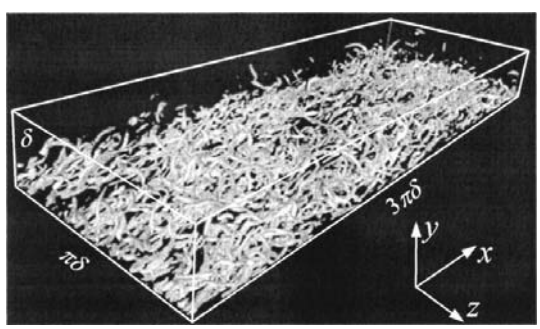

(a)

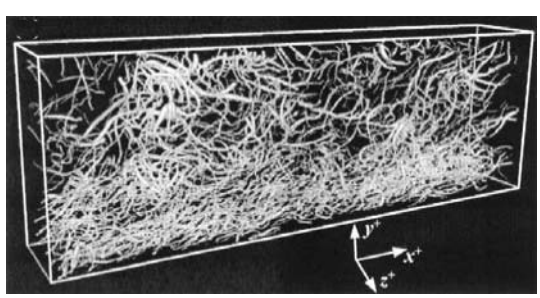

(b)

Fig. 2 (a) Contour surfaces of the second invariant Q of the velocity gradient tensor for $Re_\tau=400$ ($Q=4$). (b) Spatial distribution of the CFSE axes for $Re_\tau=800$ (domain size: $l_x^+\times l_y^+\times l_z^+=2513\times800\times400$). The diameters of the CFSE axes are drawn to be proportional to the square root of Q^*

identified. Characteristics of the detected CFSEs in turbulent channel flows can be scaled by η and u_k (Tanahashi et al., 2004; Miyauchi et al., 2005). Figure 2(b) shows spatial distribution of the CFSE axes for $Re_\tau=800$. Diameters of the CFSE axes have been drawn to be proportional to the square root of Q^* on the axes, where the superscript $*$ indicates a non-dimensional quantity scaled by $(u_k/\eta)^2$. Since the CFSEs in turbulent channel flows are scaled by η and u_k, the vortical structures could be visualized very well even in the regions far from the wall. This visualization also provides an evidence for the existence of hairpin type vortices and clusters of the CFSEs throughout the outer layer. Characteristics of the clusters of the CFSEs have been well described in Kang et al.(2004). Structures on the planes perpendicular to these CFSE axes will be discussed in the next section.

Strain rate acting on the CFSE centers is investigated in the near-wall, logarithmic and wake regions by evaluating the strain rate tensor S_{ij} $(=(\partial u_i/\partial x_j+\partial u_j/\partial x_i)/2)$ at the CFSE centers. The magnitude and direction of the local strain rates at the CFSE centers are given by eigenvalues of S_{ij} and their eigenvectors, respectively. Figure 3(a), (b) and (c) show probability density functions (pdfs) of the eigenvalues of S_{ij} in the near-wall region $(y^+<40)$, the logarithmic region $(40<y^+<200\sim450)$ and the wake region near

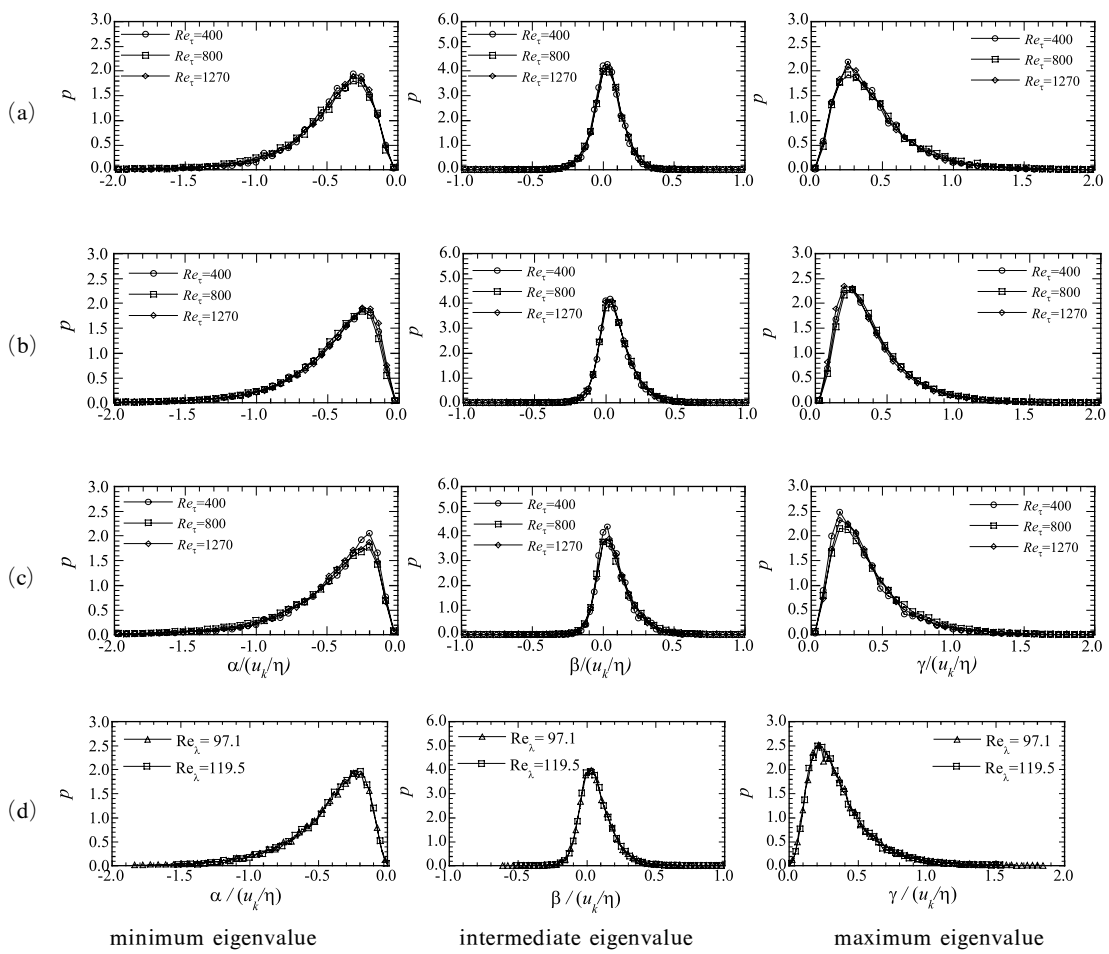

Fig. 3 Probability density functions of eigenvalues of strain rate tensor at the CFSE centers for all Reynolds number cases: (a) near-wall region, (b) logarithmic region, (c) wake region and (d) homogeneous isotropic turbulence (by using DNS data of Tanahashi et al., 2002a)

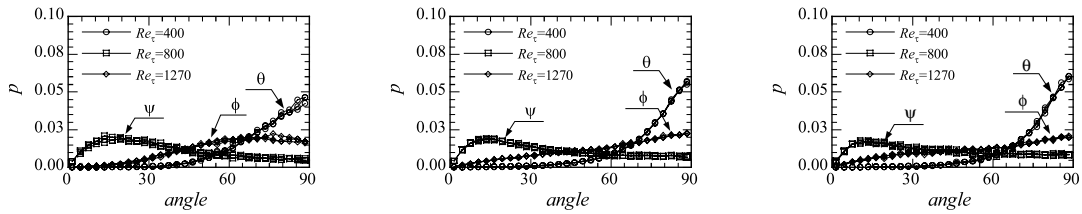

(a) (b) (c)

Fig. 4 Probability density functions of angles between unit eigenvectors corresponding to the eigenvalues and the vorticity vector at the CFSE centers for all Reynolds number cases: (a) near-wall region, (b) logarithmic region and (c) wake region

the center of the channel for all Reynolds number cases, respectively. The eigenvalues are normalized by u_k/η at y^+ where the CFSE exists. The pdfs are independent of the Reynolds number in each region of y^+. However, they have a weak y^+-dependence, especially in cases of α and γ. The pdfs of $\alpha/(u_k/\eta)$, $\beta/(u_k/\eta)$ and $\gamma/(u_k/\eta)$ in the near-wall region show peaks at about -0.32, 0.04 and 0.27 for all Re_τ, which has been early observed by DNS study of turbulent channel flow for $Re_\tau=800$ (Tanahashi et al., 2004). In the outer layer, absolute values of the most expected $\alpha/(u_k/\eta)$ and $\gamma/(u_k/\eta)$ decrease by 20～30%, which is very close to those of homogeneous isotropic turbulence in Fig. 3(d). These results suggest that the CFSE structure in the near-wall region can be different from those in the outer layer or other turbulent flows due to the large-mean shear field near the wall.

For all Reynolds number cases, Fig. 4 shows pdfs of angles between $\boldsymbol{\omega}_c$ and the eigenvectors corresponding to each eigenvalue at the CFES center in each region of y^+. θ, ψ and ϕ indicate angles between $\boldsymbol{\omega}_c$ and three unit eigenvectors $\boldsymbol{e}_\alpha$, $\boldsymbol{e}_\beta$ and $\boldsymbol{e}_\gamma$, respectively. The eigenvectors of α and γ have a tendency to be perpendicular to $\boldsymbol{\omega}_c$, especially in the outer layer. In the near-wall region, the angle (ϕ) between $\boldsymbol{\omega}_c$ and $\boldsymbol{e}_\gamma$ shows peaks at 65°～75° for all Re_τ, but it is not sharp. The most expected angles (ψ) between $\boldsymbol{\omega}_c$ and $\boldsymbol{e}_\beta$ are about 13°～23° (15°～23°: near-wall region, 13°～15°: outer region). The pdfs of each angle depend on a distance from the wall, but they are independent of the Reynolds number in each region of y^+.

4. Elliptic Feature of CFSE

Characteristics on cross sections of the CFSEs are investigated for $Re_\tau=400$ and 800 by using the phase-averaging analysis. Figure 5(a) shows contour lines of azimuthal velocity of a typical CFSE near the wall and far from the wall for $Re_\tau=800$. The radius of the displayed region in Fig. 5(a) is $2.5r_m$, where r_m denotes the radius of the CFSE. The dotted and solid lines show the

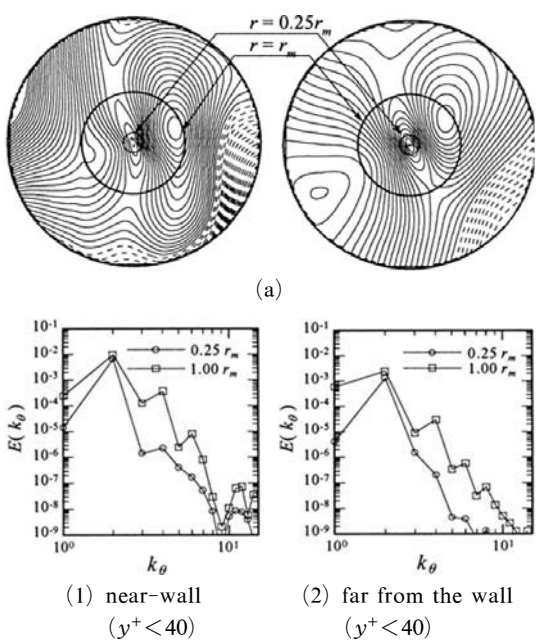

(a)

(1) near-wall ($y^+<40$) (2) far from the wall ($y^+<40$)

(b)

Fig. 5 Contour plots (a) and azimuthal energy spectra (b) of the azimuthal velocity of a typical CFSE for $Re_\tau=800$

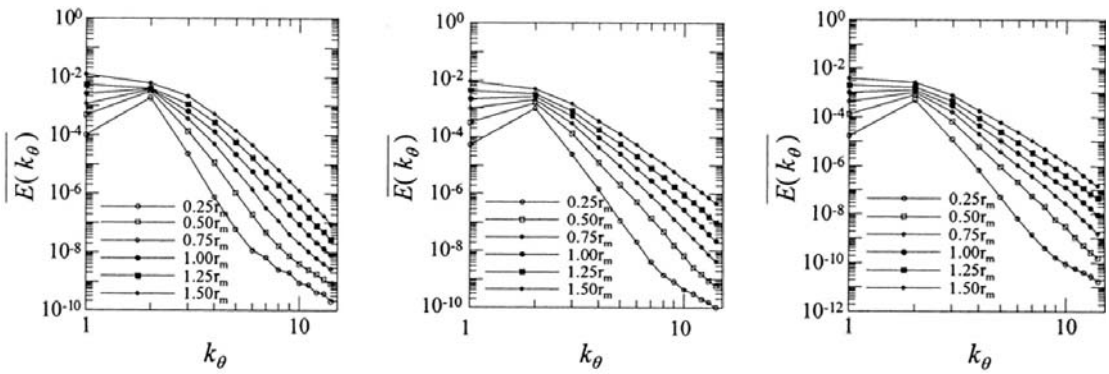

Fig. 6 Mean azimuthal energy spectra of the azimuthal velocity of the CFSE for $Re_\tau=800$

positive and negative velocity, respectively. The azimuthal velocity is defined as the relative velocity with respective to the CFSE center. Elliptic feature can be observed near the center of the CFSE, which suggests that the azimuthal velocity has a distinct character around the CFSE center. This observation is independent of a distance from the wall. Figure 5(b) shows azimuthal energy spectra of the azimuthal velocity of the typical CFSE at $r=0.25r_m$ and $r=r_m$. Here, k_θ denotes the wave number in the azimuthal direction. The Fourier transformation of the azimuthal velocity (v_θ) is given by $v_\theta(r,\ \theta)=\sum \hat{v}_\theta(r,\ k_\theta)\exp(-ik_\theta\theta)$, where $\hat{v}_\theta(r,\ k_\theta)$ is the Fourier coefficient of the azimuthal velocity for k_θ at r. The azimuthal velocity of the typical CFSE is dominated by $k_\theta=2$ mode near the center of the CFSE. In this study, the energy spectra of the azimuthal velocity of CFSEs with $D\leq 30\eta$ have been investigated to show the mean dominant mode of the azimuthal velocity.

Figure 6 shows mean azimuthal energy spectra of the azimuthal velocity (v_θ) at different locations from the CFSE center in the near-wall and outer regions. Here, v_θ is normalized with the maximum azimuthal velocity ($v_{\theta,\max}$) of each CFSE. The azimuthal velocity is dominated by $k_\theta=2$ mode near the CFSE center, which is independent of a distance from the wall and the Reynolds number. The energy at each k_θ mode tends to increase with the increase of r, which is prominently observed in $k_\theta=1$ mode. On the other hand, the rate of increase in the energy at $k_\theta=2$ mode is very low compared with those in other modes. This result is also independent of a distance from the wall and the Reynolds number. Therefore, the phase-averaging analysis is conducted based on $k_\theta=2$ mode of v_θ at $r=0.25\ r_m$.

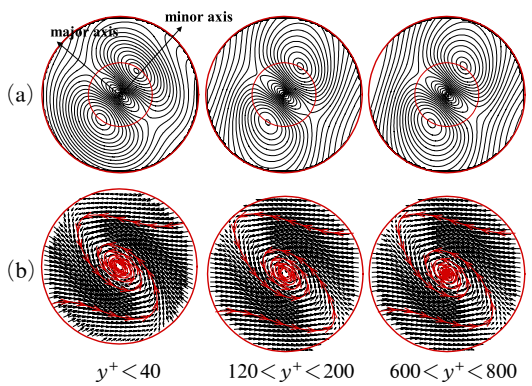

Fig. 7 Contour plots of the phase-averaged azimuthal velocity (a) and vector plots of the phase-averaged velocity (b) and around the CFSEs for $Re_\tau=800$

Figure 7 shows contours of the phase-averaged $v_\theta^*/v_{\theta,\max}^*$ and velocity vectors with streamlines, respectively. The superscript $*$ indicates a non-dimensional quantity scaled by u_k. Note that the velocity vectors are constructed from the azimuthal and radial velocity components. Elliptic feature of the CFSE is observed in contours of the phase-averaged azimuthal velocity near the

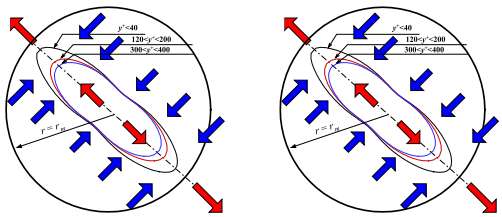

Fig. 8 Iso-lines of the phase-averaged azimuthal velocity ($v_\theta^*/v_{\theta,\max}^*=0.5$) near the CFSE center in the near-wall region and the outer layer for $Re_\tau=400$ (a) and 800 (b)

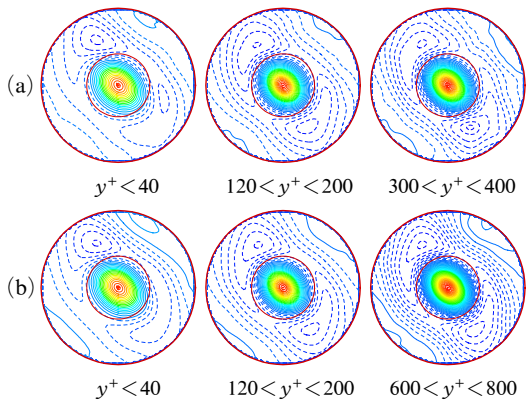

Fig. 9 Contour plots of the phase-averaged second invariant Q^* on the plane perpendicular to the CFSE axis for $Re_\tau=400$ (a) 800 (b)

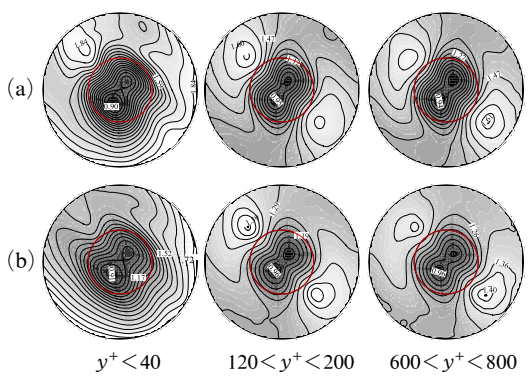

Fig. 10 Distributions of the phase-averaged α^*/α_c^* and γ^*/γ_c^* around the CFSEs for $Re_\tau=800$

CFSE center and in streamlines of the velocity vectors independent of a distance from the wall, whereas the elliptic shape has a weak y^+-dependence. The elliptic shape in the near-wall region is more compressed compared with those in the outer layer, which is clearly observed in Fig. 8. Figure 8 shows iso-lines of $v_\theta^*/v_{\theta,\max}^*=0.5$ in the near-wall region and in the outer layer for $Re_\tau=400$ and 800. The ellipticity is larger in the near-wall region than in the outer layer, which suggests that the CFSE is obtaining the effect of the strong mean shear stress near the wall. The elliptic feature has also been observed in homogeneous isotropic turbulence (Miyauchi et al., 2002), and confirmed by measurements of PIV in turbulent mixing layer (Tanahashi et al., 2002b). Distributions of the radial velocity, which are not shown here, show existence of distinct inflow into and outflow from the CFSE center.

Figure 9 shows contour plots of the phase-averaged Q^* ($=Q/(u_k/\eta)^2$) for $Re_\tau=400$ and 800. Dotted and solid lines indicate the negative and positive Q^*. Distributions of the phase-averaged Q^* show maxima at the CFSE center and minima on the major axis around the CFSE, which coincides with the fact that the CFSE center exists near the $Q_{\max}$ point. The contour lines of Q^* near the CFSE center also show elliptic feature for all y^+ regions.

Figure 10 shows contours of the phase-averaged compressing eigenvalue (α^*/α_c^*) and stretching eigenvalue (γ^*/γ_c^*) in each y^+ region. The superscript $*$ indicates a non-dimensional quantity scaled by u_k/η, and the subscript c denotes the CFSE center. Far from the wall, α^*/α_c^* and γ^*/γ_c^* show two symmetric maxima at about $1.4\sim1.6r_m$ on the major axis and two symmetric minima at about $0.5\sim0.6r_m$ on the minor axis, while they have no distinct maxima in the near-wall region and the values of α^*/α_c^* and γ^*/γ_c^* around the CFSE become larger than those in the outer layer. These results indicate that larger compression and stretching are acting around the CFSEs compared with on the CFSE centers. Except for the near-wall region, these distributions are similar to those of the phase-averaged dissipation rate of kinetic energy in homogeneous isotropic turbulence (Miyauchi et al., 2002).

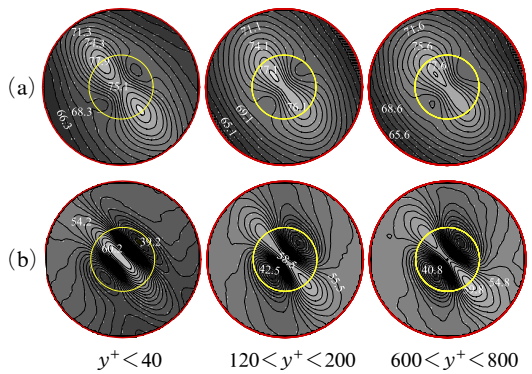

Fig. 11 Distributions of the phase-averaged angles between the vorticity vector at the CFSE center and unit eigenvectors $\boldsymbol{e}_\alpha$ (a) and $\boldsymbol{e}_\gamma$ (b) on cross sections of the CFSEs for $Re_\tau=800$

These results are independent of the Reynolds number. The phase-averaged intermediate eigenvalue (β^*/β_c^*) on the cross section of the CFSE, which is not shown here, shows the irregular distributions because the values of β^* are very small and the signals of β^* have positive or negative irregularly.

Distributions of the phase-averaged angels between $\boldsymbol{\omega}_c$ and eigenvectors of α and γ on cross sections of the CFSEs are shown in Fig. 11. The interval of contour lines is 1.0° for both, and ranges of the phase-averaged θ and ϕ are 65°～78° and 39°～61°, respectively. The θ and ϕ on the major axis are larger than those on the minor axis and are almost equal to those at the CFSE center (i.e. $\theta=78°\sim70°$ and $\phi=55°\sim50°$), which is also independent of the Reynolds number. These results suggest that directions of the stretching and compression on the minor axis are hard to be perpendicular to the rotating axis of the CFSE compared with those on major axis.

5. Conclusions

In the present study, strain rate field and elliptic feature of the CFSEs in wall turbulence were statistically investigated by using DNS data of turbulent channel flows. The principal strain rates at the CFSE centers in the near-wall, logarithmic and wake regions are scaled by u_k/η up to $Re_\tau=1270$. By using a phase-averaging analysis, elliptic feature on cross sections of the CFSEs has been investigated in the near-wall region and the outer layer. As results, the following conclusions are obtained in the present study.

(1) The most expected CFSEs in the near-wall region $(y^+<40)$ suffer about 20～30% stronger compression and stretching at their center compared with those in the outer layer. Directions of each eigenvalues corresponding to the rotating axis of the CFSEs are independent of the Reynolds number in the near-wall, logarithmic and wake region. This tendency is independent of the Reynolds number.

(2) The CFSEs in wall turbulence possess elliptic features on their cross sections similar to those in other turbulent flows. However, the ellipticity in the near-wall region is larger than that in the outer layer due to the strong mean shear or wall effects.

(3) On the major axis of the CFSE, there are two regions with large compression and stretching. These regions contribute to the high energy dissipation rate around the CFSEs.

References

Ashurst, W. T., Kerstein, A. R., Kerr, R. M. and Gibson, C. H., 1987, "Alignment of Vorticity and Scalar Gradient with Strain Rate in Simulated Navier-Stokes Turbulence," *Phys. Fluids*, Vol. 30, pp. 2343～2353.

Blackburn, H.M., Mansour, N.N. and Cantwell, B. J., 1996, "Topology of Fine-scale Motions in Turbulent Channel Flow," *J. Fluid Mech.*, Vol. 310, pp. 269～292.

Hunt, J. C. R, Wray, A. A. and Moin, P., 1988, "Eddies, Stream and Convergence Zones in Turbulent Flows," *Center for Turbulence Research Report*, CTR-S88, pp. 193.

Jimenez, J. and Wray, A. A., 1998, "On the Characteristics of Vortex Filaments in Isotropic Turbulence," *J. Fluid Mech.*, Vol. 373, pp. 255～285.

Jimenez, J., Wray, A. A., Saffman, P. G. and Rogallo, R. S., 1993, "The structure of Intense

Vorticity in Isotropic Turbulence," *J.Fluid Mech.*, Vol. 255, pp. 65～90.

Kang, S. -J., Tanahashi, M. and Miyauchi, T., 2004, "Coherent Fine Scale Eddies and Large-scale Structures in wall Turbulence," *Advances in Turbulence X*, pp. 603～606.

Kim, J., Moin, P. and Moser, R. D., 1987, "Turbulence Statistics in Fully Developed Channel Flow at Low Reynolds Number," *J. Fluid Mech.*, Vol. 1777, pp. 133～166.

Mansour, N. N., Kim, J. and Moin, P., 1988, "Reynolds-stress and Dissipation-rate Budgets in a Turbulent Channel Flow," *J. Fluid Mech.*, Vol. 194, pp. 15～44.

Miyauchi, T., Tanahashi, M., Takata, N. and Iwase, S., 2002, "Scalar Dissipation Rate and Coherent Fine Scale Eddies in Turbulence," *Proc. Int Symp. Dynamics and Statistics of Coherent Structures in Turbulence : Roles of Elementary Vortices*, Tokyo Japan, pp. 249～258.

Miyauchi, T., Kang, S. -J. and Tanahashi, M., 2005, "Coherent Fine Scale Eddies in the Logarithmic Region of Turbulent Channel Flows," *Proc. IUTAM Symp. Elementary Vortices and Coherent Structures, Fluid Mechanics and Applications*, Kluwer Academic Publishers, in print.

Orszag, S. A., 1971, "Numerical Simulation of Incompressible Flows with Simple Boundaries," *Stud. Appl. Math.*, Vol. 50, pp. 293～327.

Prochazka, A. and Pullin, D. I., 1998, "Structure and Stability of Non-symmetric Burgers Vortices," *J. Fluid Mech.*, Vol. 363, pp. 199～228.

Soria, J., Sondergaard, Cantwell, B. J., Chong, M. S. and Perry, A. E., 1994, "A Study of the Fine-scale Motions of Incompressible Time-developing Mixing Layers," *Phys. Fluids*, Vol. 6, pp. 871～884.

Tanahashi, M., Miyauchi, T. and Yoshida, T., 1996, "Characteristics of Small Scale Vortices Related to Turbulent Energy Dissipation," *Proc. 9th International Symposium on Transport Phenomena*, Vol. 2, pp. 1256～1261.

Tanahashi, M., Miyauchi, T. and Matsuoka, K., 1997, "Coherent Fine Scale Structure in Temporally Developing Turbulent Mixing Layers," *Proc. 2nd Int. Symp. on Turbulence, Heat and Mass Transfer*, Vol. 2, pp. 451～470.

Tanahashi, M., Miyauchi, T. and Ikeda, J., 1999, "Identification of Coherent Fine Scale Structure in Turbulence," *Proc. IUTAM Symp., Fluid Mechanics and Applications*, Vol52, Kluwer Academic Publishers, pp. 131～140.

Tanahashi, M., Iwase, S. and Miyauchi, T., 2001, "Appearance and Alignment with Strain Rate of Coherent Fine Scale Eddies in Turbulent Mixing Layer," *J. of Turbulence*, 2, No. 6.

Tanahashi, M., Tsukamoto, Y., Iwase, S. and Miyauchi, T., 2002a, "Coherent Fine Scale Eddies and Energy Cascade in Homogeneous Isotropic Turbulence," 2002a, *Proc. Int Symp. Dynamics and Statistics of Coherent Structures in Turbulence : Roles of Elementary Vortices*, Tokyo Japan, pp. 259～268.

Tanahashi, M., Ootsu, M., Fukushima, M. and Miyauchi, T., 2002b, "Measurement of Coherent Fine Scale Eddies in Turbulent Mixing Layer by DPIV," *Engineering Turbulence Modeling and Measurements*, Vol. 5, pp. 525～534.

Tanahashi, M., Kang, S. -J., Miyamoto, T., Shiokawa, S. and Miyauchi, T., 2004, "Scaling Law of Fine Scale Eddies in Turbulent Channel flows up to Re_τ=800," *Int. J. Heat and Fluid Flow*, Vol. 25, pp. 331～340.